InfraStructs: Fabricating Information Inside Physical Objects for Imaging in the Terahertz Region

Karl D.D. Willis
Carnegie Mellon University

Andrew D. Wilson
Microsoft Research

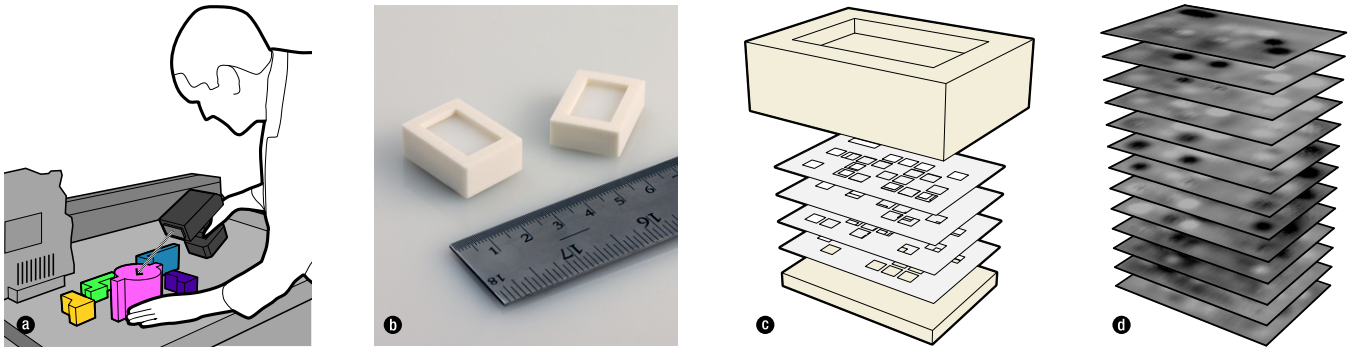

Figure 1: *InfraStructs are material-based tags that embed information inside physical objects for imaging in the Terahertz region. Terahertz imaging can safely penetrate many common materials, opening up new possibilities for encoding hidden information inside digitally fabricated objects. (a) InfraStruct tags are embedded during the fabrication process to immediately identify objects without additional labeling or packaging. (b) Inexpensive polymer materials are used to (c) create a layered internal structure. (d) The object interior is scanned to create a volumetric image that is decoded into meaningful information.*

Abstract

We introduce *InfraStructs*, material-based tags that embed information inside digitally fabricated objects for imaging in the Terahertz region. Terahertz imaging can safely penetrate many common materials, opening up new possibilities for encoding hidden information as part of the fabrication process. We outline the design, fabrication, imaging, and data processing steps to fabricate information inside physical objects. Prototype tag designs are presented for location encoding, pose estimation, object identification, data storage, and authentication. We provide detailed analysis of the constraints and performance considerations for designing *InfraStruct* tags. Future application scenarios range from production line inventory, to customized game accessories, to mobile robotics.

CR Categories: I.3.6 [Computer Graphics]: Methodology and Techniques—Interaction techniques I.4.1 [Image Processing and Computer Vision]: Digitization and Image Capture—Scanning

Keywords: Digital fabrication, terahertz, THz, imaging, sensing, data, encoding, 3D printer, laser cutter, materials.

Links: DL PDF WEB

ACM Reference Format
Willis, K., Wilson, A. 2013. InfraStructs: Fabricating Information Inside Physical Objects for Imaging in the Terahertz Region. ACM Trans. Graph. 32, 4, Article 138 (July 2013), 10 pages.
DOI = 10.1145/2461912.2461936 http://doi.acm.org/10.1145/2461912.2461936.

DOI: http://doi.acm.org/10.1145/2461912.2461936

1 Introduction

Computer-controlled digital fabrication technologies are rapidly changing how objects are manufactured. Both additive (e.g., 3D printing) and subtractive (e.g., laser cutting) techniques use digital information to programmatically control the fabrication process. Unlike conventional manufacturing, one individual object can differ significantly from the next. The ability to manufacture one-off objects has implications not only for product customization and on-demand manufacturing, but also for tagging objects with individualized information.

Object tagging systems have wide-ranging uses in logistics, point of sale, robot guidance, augmented reality, and many other emerging applications that link physical objects with computing systems. 1D and 2D barcodes have been successful due to their low cost, but are limited by their obtrusive appearance that is visible to the human eye. Radio Frequency Identification (RFID) tags can be embedded inside objects but typically require electronic components beyond the capabilities of current digital fabrication technologies. As the number of digital fabricated objects increase, how can unobtrusive information be tagged to these objects *during* the manufacturing process?

We introduce a novel volumetric tag design, called an *InfraStruct*, which embeds information in the interior of digitally fabricated objects and is read using a Terahertz (THz) imaging system (Figure 1). *InfraStructs*, literally meaning 'below structures', are material structures that are not visible to the eye but can be clearly imaged in the THz region. By modulating between materials information can be encoded into the volumetric space inside objects. THz imaging is ideally suited to reading material transitions due to its ability to see through many materials used with digital fabrication. Common and inexpensive polymer materials can be used with both additive and subtractive digital fabrication technologies to embed tags directly inside physical objects. Both machine-readable digital information, and human-readable visual information can be embedded to support many application scenarios.

We introduce the concept of pairing modulated material structures inside digitally fabricated objects with THz imaging to sense material transitions. Our approach enables arbitrary information to be encoded and decoded from entirely within physical objects. We present the following contributions:

- Techniques for constructing machine-readable tags inside physical objects using digital fabrication.
- Techniques for sensing, interpreting, and processing THz imaging data to extract tag information.
- Prototype tag designs including Gray codes for location encoding, geometric structures for pose estimation, random voids for object identification, matrices for data storage, and visual data for object authentication.
- Detailed system design, discussion, and evaluation to demonstrate future application scenarios for *InfraStruct* tags.

We show that THz imaging is well-suited to sensing the physical structures generated with digital fabrication. To the best of our knowledge this work is the first to approach embedding information inside digitally fabricated objects. We envision these objects being used in applications ranging from simple inventory control to real-time game interaction. This work opens up new possibilities for the design and manufacture of highly customized physical objects already embedded with machine-readable information.

2 Related Work

The need to tag objects with machine-readable information is a well established requirement of ubiquitous computing [Weiser 1993] and has given rise to a number of solutions in both the radio frequency (RF) and optical domains. THz radiation benefits from its unique location *between* the RF and optical wavelengths on the electromagnetic (EM) spectrum. In this section we compare THz imaging to other approaches in the surrounding areas of the EM spectrum and discuss work related to tag fabrication.

Comparison with RF Approaches: Tag systems utilizing RF have the ability to penetrate a range of materials [Hashemi 1993], but provide limited spatial resolution for imaging due to their longer wavelengths. Although ultrawideband radar has been used for see-through-wall imaging [Yang and Fathy 2005], forming an accurate image from reflected radar waves is the subject of ongoing research. Radio Frequency Identification (RFID) tags typically consist of an antenna and integrated circuit powered by an active reader. RFID approaches can provide some localization data based on radio signal strength information [Hightower et al. 2000], but are imprecise due to a lack of directionality. RFID tags have been coupled with optical sensing to improve spatial localization [Raskar et al. 2004]. Unlike RF approaches, THz frequencies enable high resolution volumetric imagery to be accurately sensed from precise locations inside an object. Information can be encoded in either machine-readable *digital* or human-readable *visual* form.

Comparison with Optical Approaches: Optical imaging with visible and near-IR light provides high spatial resolution but cannot penetrate visibly opaque materials. Both 1D and 2D barcodes rely on line of sight to be detected and are sensitive to changing lighting conditions [Kato and Tan 2007]. Barcode tags are typically visible to the human eye and have an obtrusive geometric appearance. Time of flight (TOF) depth cameras could potentially be used to read encoded depth information on the first, or even second [Velten et al. 2012], surface of objects they encounter. However, information about internal surfaces can not be detected using visible/IR emission sources. When compared with other optical approaches, THz imaging is unique in its ability to see *inside* objects and sense material transitions. THz imaging is related to 'millimeter wave' technologies used in full-body scanners commonly found in airports. However, due to shorter wavelengths, higher resolution images can be achieved in a much more compact form-factor.

Tag Fabrication: New tools and uses for digital fabrication are rapidly being explored [Bächer et al. 2012; Bickel et al. 2010; Stava et al. 2012; Willis et al. 2012]. Techniques for embedding spatial information in digitally fabricated objects have to date focused on surface geometry [Alexa and Matusik 2010; Aliaga and Atallah 2009; Chao and Aliaga 2013; Hašan et al. 2010; Weyrich et al. 2009]. We are unaware of any prior work that allows machine-readable tags to be embedded *inside* of a digitally fabricated object. Although most RFID tags use integrated circuits, chip-less printable tags have been demonstrated with inkjet-printable transistors [Subramanian et al. 2005] and passive spiral resonators [Yang et al. 2007]. Although promising, integration of printed electronics with digital fabrication is still in the early research stages [Lopes et al. 2012]. Initial work using chip-less RFID tags in the THz frequencies has been explored with dielectric materials in a Bragg structure [Bernier et al. 2011]. Our approach encodes information in the time domain, rather than the frequency domain used by RFID. A number of unique materials have been used to conceal optical barcode tags from the human eye. These include transparent retroreflective films [Nakazato et al. 2008], lenslets arrays [Mohan et al. 2009], and IR-absorbing inks [Park and Park 2004]. The use of specialized materials, however, greatly limits the ease of fabrication. By using common polymer materials, *InfraStructs* can be fabricated on a range of standard equipment.

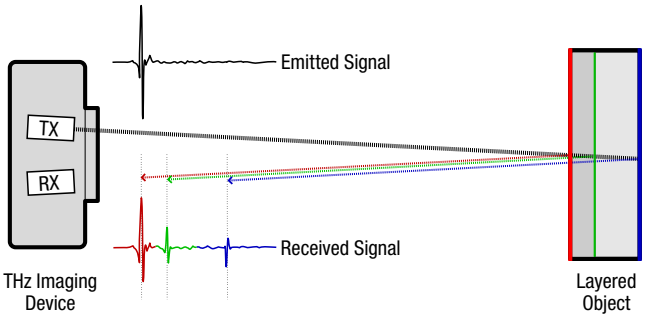

Figure 2: *THz TDS systems emit a pulse of THz radiation and measure reflections from material interfaces encountered on the outer and inner surfaces of an object.*

3 THz Imaging

THz imaging constructs volumetric intensity, depth, and spectral images of the *surface* and *interior* of physical objects. We now briefly introduce the properties of THz radiation and time-domain spectroscopy. In-depth information on THz technology can be found in several review papers [Chan et al. 2007; Tonouchi 2007].

3.1 THz Radiation

The THz band of the electromagnetic (EM) spectrum lies between microwaves and infrared (IR) light. This so-called 'THz gap' is typically classified between 0.1–10 THz (λ = 3000–30 μm). A relative lack of convenient and inexpensive THz emitters and detectors left the THz band relatively unexplored up until the 1970s. THz radiation can penetrate many common plastics, papers, and textiles [Chan et al. 2007]. Although X-rays have similar capabilities, THz radiation is a non-ionizing, safer alternative with power emission on the μW level.

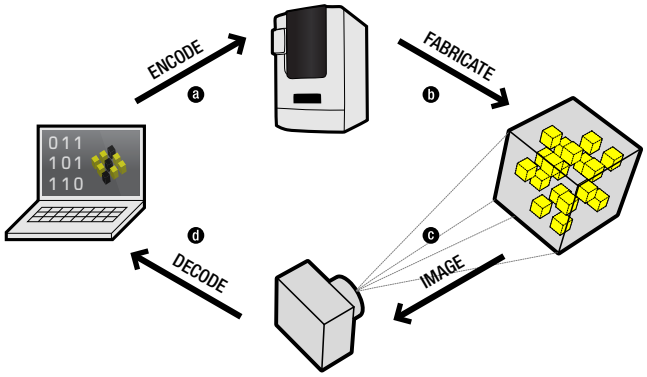

Figure 3: *InfraStructs are created by (a) encoding information into a digital model that is then (b) fabricated with material transitions inside a physical object. The object's internal volume is (c) imaged in the THz region and (d) decoded into meaningful information.*

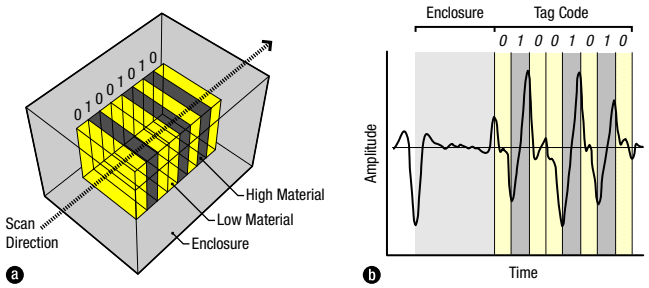

Figure 4: *(a) Internal material structure of a simple InfraStruct tag. (b) The reflected THz TDS signal shows peaks at the interfaces between materials that are decoded into binary form.*

3.2 Time-Domain Spectroscopy

The most common approach to THz imaging has to date been *Time-Domain Spectroscopy* (TDS) [Auston and Cheung 1985]. Similar to time-of-flight (TOF) depth cameras, TDS systems perform active illumination and measure the signal reflected back from the scene. Rather than measuring only the flight time of the signal, TDS systems emit a broadband pulse of THz radiation and measure the entire reflected signal as a waveform (Figure 2). Each 'pixel' in a TDS image consists of a time-domain signal with peaks that indicate reflected energy from both the *outer* and *inner* surfaces of objects in the scene. The entire image forms a volumetric dataset that can be used to slice through an object along the depth axis and reveal the 3D structure (Figure 1d). Until recently THz imaging devices were not capable of interactive scan rates, leaving a vast array of possibilities unexplored. Volumetric data acquisition for TDS systems is still relatively slow, but real-time line-scan systems are commercially available and tomographic imaging can also be used [Wang and Zhang 2004]. Although other forms of THz systems do exist, e.g., *continuous-wave* systems [Kleine-Ostmann et al. 2001], we use TDS systems due to the richer dataset generated. The remainder of the paper deals with TDS systems exclusively.

4 InfraStructs

InfraStructs use digital fabrication techniques to embed information inside objects and THz imaging to later decode this information. Figure 3 shows a conceptual overview of how *InfraStructs* are encoded, fabricated, imaged, and decoded. (a) Information is encoded in a digital model to create structured transitions between materials. (b) Digital fabrication is used to precisely manufacture the digital model with material transitions enclosed internally. (c) A THz TDS system is used to create a volumetric image of the object interior. (d) The volumetric image is processed to decode the embedded structures into meaningful information.

4.1 Overview

InfraStructs can be used to encode information in numerous ways. Before we introduce individual tag designs, we start by providing an illustrative example of a simple 1D tag used to encode eight bits of binary information (Figure 4a). This tag consists of two modulated materials surrounded by an outer enclosure. The 'high material' has a higher refractive index and represents a high (1) binary state. The 'low material' has a lower refractive index and represents a low (0) binary state. The THz TDS scan occurs perpendicular to the internal code, reflecting a signal at each material interface. Figure 4b illustrates the returned signal from a single scan through the structure. The scan first passes through the enclosure material, reflecting a negative peak as it enters a material with a higher refractive index, then a positive peak as it transitions to a material with a lower refractive index. Similar positive-negative peak pairs occur as the scan passes through each layer of high material embedded within the tag itself. The full signal is decoded into binary form by comparing the timing of peaks to the known tag structure and material refractive index. Using this procedure, binary information can be encoded simply by varying the material structures within a physical object. We now outline the technical factors that govern the fabrication, imaging, and design of *InfraStruct* tags.

4.2 Material Model

Material selection is a key consideration that determines the strength of reflected signals and the degree of material penetration. We model material performance for a tag based on two factors: *reflected* radiation – the amount of radiation reflected at the interface between two materials, and *transmitted* radiation – the amount of radiation transmitted after attenuation through a material.

Assuming normal incidence, the amount of reflected radiation, r, is calculated using the refractive index of the current material, n_1, and the refractive index of the material into which the radiation will enter, n_2:

$$r = \left(\frac{n_1 - n_2}{n_1 + n_2}\right)^2 \tag{1}$$

Non-reflected radiation will continue to pass through to the next material. The amount of radiation transmitted through a material, t, is given by:

$$t = se^{-ab} \tag{2}$$

where a is the material absorption coefficient, b is the thickness of the material, and s is the input radiation. The signal returned from the last layer encounters the most signal loss. For a structure with i layers, the end layer will encounter $4i - 3$ signal losses due to reflections at each layer interface and $2i - 2$ signal losses due to attenuation through each layer. Here we assume material interfaces at each layer, even with consecutive material layers.

An *InfraStruct* tag design should aim to minimize t by selecting materials that have a low absorption coefficient in the THz region and minimal thickness. An appropriate r value should be based on the number of layers. With fewer layers, a higher difference in refractive index between materials is preferred to produce a stronger signal. However with more layers, a lower difference in refractive index allows a greater portion of the signal to reach the end layer of

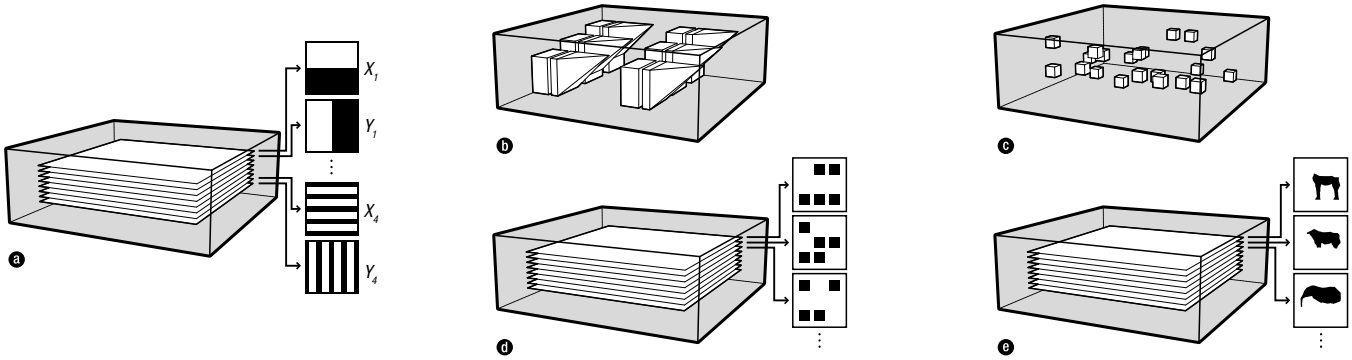

Figure 5: *Prototype designs for InfraStruct tags including (a) Gray code, (b) geometric, (c) random void, (d) matrix, and (e) visual designs.*

the code. In practice, *air* can be used as the low material to increase the difference in refractive index and maximize r.

4.3 Decoding Algorithm

Once a tag has been modeled, fabricated, and scanned, we use a custom algorithm to convert the THz time domain data to the spatial-domain and decode the tag structure. The time domain data reveals the 'optical distance' between materials – the product of the distance the radiation has travelled and the refractive index of the medium it travelled through. Conversion from optical distance to real-world distance forms the basis of identifying material structures within an *InfraStruct* tag. Optical distance, d, can be converted into real-world distance:

$$d = \frac{tnc}{2} \tag{3}$$

Here t is the time taken for the radiation to travel some distance, n is the refractive index of the medium, and c is the constant speed of light in a vacuum. As the time measurements are based on reflection, i.e., a two-way journey, the final value must be divided by two to calculate the real-world distance. To identify the sequence of materials inside an object we require two basic pieces of information: material layer thickness, b, and refractive index, n. This allows the optical thickness of both materials to be pre-calculated. Additionally, it is useful to know the location of the tag within the object and the number of tag layers, but these factors do not affect the basic functionality of our decoding algorithm.

Our decoding algorithm (Algorithm 1) takes advantage of the clear sequence of peaks in the returned time domain data. The first peak occurs as the signal travels from air into the outer enclosure, creating a negative peak. As the signal transitions out of the enclosure it generates a positive peak that acts as a starting point, p, to search for further peaks within the tag itself. We iteratively search for negative peaks at a given offset from p, determined by the optical thickness of the high material. If we find a peak over a given threshold it indicates there is a high material layer present. If there is no peak present we assume a low material layer. This process is repeated until all layers are decoded into a sequence of bits representing the embedded signal. This basic algorithm is optimized for tag structures that have an interface between each material layer. Slight variations of the algorithm can support different structures and we discuss the benefits of various fabrication approaches later in the paper.

Algorithm 1 *InfraStruct* Decoding

```
outerSurface = findNegativePeakAfter(0)
innerSurface = findPositivePeakAfter(outerSurface)
p = innerSurface     // search start point
h = b1n1c     // high material optical thickness
l = b0n0c     // low material optical thickness

for each layer i do
   peak = findNegativePeak(p + h, windowSize)
   if peak then
      p = peak
      code[i] = 1     // high material
   else
      p = p + l
      code[i] = 0     // low material
   end if
end for
```

4.4 Designs

InfraStructs tags can encode information in numerous ways. We have developed five prototype tag designs that demonstrate the different types of information and methods of encoding (Figure 5). Each tag design is targeted towards a specific THz imaging configuration. The a) ray scan, b) planar scan, and c) volume scan configurations represent the 1D, 2D, and 3D datasets respectively (Figure 6). We attempt to maximize the level of information that can be extracted with minimal data dimensions. As THz imaging devices advance, we expect to be able to utilize increasingly sophisticated THz scanning configurations. Each tag design has unique advantages/limitations and the right choice of tag will depend on the specific application.

Gray Code: Sensing tag location is a key component of many ubiquitous computing applications. Understanding the precise location of physical objects enables interaction with nearby devices and digital content. Spatial Gray code patterns have been used to resolve location by displaying a sequence of binary patterns over time [Salvi et al. 2004]. Reading this sequence of binary values at any given location within the pattern results in a binary code that is unique to a spatial location. Based on this principle, we introduce an *InfraStruct* tag design for determining location using a multi-

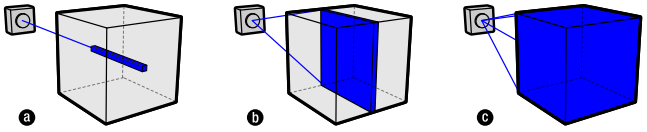

Figure 6: *Prototype tags designs use (a) ray scan, (b) planar scan, and (c) volume scan configurations for a THz imaging system.*

layered Gray code pattern (Figure 5a). We encode Gray codes patterns into material layers within an object. Using only a ray scan configuration, XY location can be decoded based on the sequence of material layers encountered. Additionally, the z depth value can be extracted based on TOF to the object surface.

Geometric: Pose estimation can be achieved with a number of different sensing modalities. THz imaging enables an alternative form of pose estimation by looking inside objects to reveal structural information. Internal geometry within an object can be designed to reflect unique signals based on how they are positioned and oriented. We introduce a proof-of-concept tag design with embedded geometric structures (Figure 5b) designed to be read with a planar scan configuration. When scanned from above, a 2D image is generated that cuts through the object and reflects distinct signals from the geometric structures inside. The design of the internal geometry can be tailored to the specific degrees of freedom required.

Random Void: The ability to uniquely identify a visibly homogenous object is important for a variety of application scenarios. Random physical structures have qualities that make them well suited to object identification [Pappu et al. 2002]. We introduce a combined pose estimation/object identification technique using randomly placed THz-detectable features under the surface of an object (Figure 5c). When scanned, the random features function as a unique fingerprint that can be matched to a stored 3D model containing the position of all features in the object. Due to the distributed nature of the random features, the main requirement is to capture a sufficient number of features so the identity and pose of the object can be uniquely determined. Either a planar or volume scan are used depending on feature density. One possible advantage of this technique is the creation of generic materials that can be cut into multiple pieces without affecting the matching process.

Matrix: Storing data inside physical objects is useful for a range of applications and numerous schemes have been developed. In contrast to our Gray code tag design that uses a single ray scan, we introduce a matrix tag design that embeds data in the volumetric space of an object (Figure 5d). The matrix tag contain layers of digital information encoded as physical bits and imaged using a volume scan configuration. To read all bits requires at least one TDS signal for each data point in the XY plane.

Visual: THz volume scans can be used to encode visual information beneath the surface of objects. Although the surface material may be opaque, arbitrary shapes and patterns can be hidden inside an object. Human-readable 'watermarks' have applications in security to verify the authenticity of an object or in consumer products to provide the customer with proof that the object is not counterfeit. The embedded information can be easily recognized by a human provided they have the right equipment and know the information location. We introduce a visual tag design that embeds graphical shapes inside an object to form a 3D watermark (Figure 5e). Each layer represents a parallel slice of a 3D object and is fabricated from multiple layers of material. A volume scan configuration is used to image the entire layer set.

5 Implementation

We now describe the techniques used to fabricate and image *InfraStruct* tags and present implementation details and results from our prototype tag designs.

5.1 Fabrication

InfraStructs can range from thin film-like layers to volumetric structures that fill entire objects. Figure 7 shows prototype objects

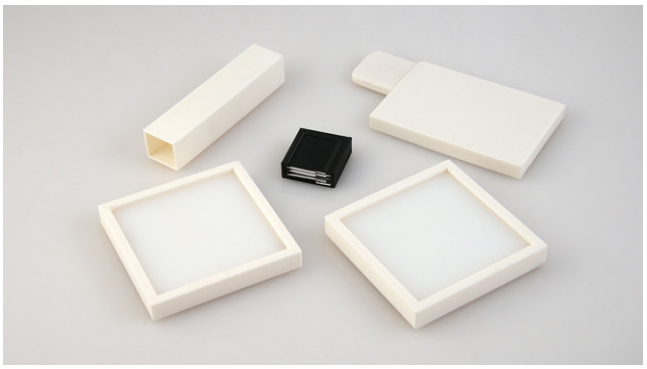

Figure 7: *Sample InfraStruct objects used in our experiments.*

with embedded *InfraStruct* tags. To maximize the return signal we select materials with high transparency in the THz region for use as the high material and use air as the low material. This approach enables *InfraStruct* tags to be fabricated using both additive and subtractive fabrication techniques – both have advantages and limitations depending on the type of tag.

Additive: Additive manufacturing, or 3D printing, enables physical objects to be formed by selectively adding material layer by layer. Unlike conventional manufacturing methods, the additive process enables complex internal geometry to be fabricated. Interlinked, nested, and enclosed geometries can be fabricated, but require support material removal. Support material is a sacrificial material that provides structural support for overhanging or hollow areas of a model. Support material is typically removed after fabrication but can also become trapped inside of enclosed areas. Because *InfraStruct* tags utilize the internal space within objects, removing support material allows for hollow areas with highly reflective material transitions from material–air and air–material.

Using additive fabrication there are several ways to create hollow internal areas for use with *InfraStructs* tags. One approach is to use self-supporting geometry where a small amount of step-over (overhang) from layer to layer allows hollow areas to be slowly closed. This approach is efficient because it does not require post-processing, but it does place limits on the type of geometry that can be fabricated. Fused deposition modeling (FDM) 3D printers allow for a fairly substantial step-over and smaller step-overs are possible with material-jetting 3D printers [Willis et al. 2012]. A second solution is to leave openings in the model that allow for support material to be removed; we use this approach when creating geometric tag designs. A third approach is to create a model in two pieces, remove support, then bond them together; we use this approach when creating random void tag designs.

Multi-material 3D printers can also be used to design complex internal structures using a secondary material. Although materials with disparate softness and color can be fabricated side by side, many of the commercially available materials have similar refractive index values. In the Discussion section we analyze the THz transmission properties of common 3D printer materials. We also note our observations about how THz radiation interacts with micro-scale structures from multi-material and FDM 3D printers.

Subtractive: Subtractive manufacturing encompasses a broad range of technologies that subtract (i.e., cut) from a raw material to form a desired shape. Laser cutters, vinyl cutters, and computer numerical control (CNC) mills in particular, although originally used in industrial settings, have become increasingly accessible due to the convenience of computer controlled fabrication.

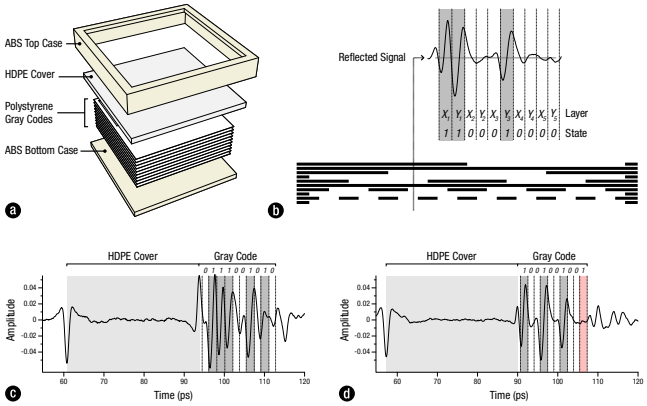

Figure 8: *(a) Gray code patterns are encoded into layers of material inside a physical object. (b) Using only a single THz ray scan an x,y coordinate can be decoded from the reflected signal. (c) A successfully decoded signal. (d) A signal with a single error in a lower-order bit is still resolvable to a lower resolution coordinate.*

We fabricate the Gray code, matrix, and visual tag designs from layers of polystyrene or high density polyethylene (HDPE) cut with a CO_2 laser cutter by Universal Laser Systems. These materials are selected due to their refractive index and absorption coefficient properties – both materials are highly transparent in THz and also very inexpensive. The material layers are enclosed in 3D printed Acrylonitrile butadiene styrene (ABS) cases to ensure accurate alignment. Layer thicknesses down to 127 µm allow for thin film-like tags to be created. Material layers are packed tightly, but not physically bonded, allowing clear signal reflections to be achieved at each material interface.

5.2 Imaging

We analyze the prototype tag designs by firstly scanning them with a THz TDS system and then processing the resulting data.

Scanning: We use a Picometrix® T-Ray 4000® system (`www.picometrix.com`) to scan each tag design. The T-Ray 4000® system can be used in the three configurations shown in Figure 6. All scans are performed in reflection mode (Figure 2). The ray scan configuration consists of a stationary THz emitter-receiver pair mounted from above. Real-time data is recorded at up to 100 Hz on an attached computer. Each signal consists of 4096 samples with a resolution of 0.078 ps, equating to a depth resolution of 23.4 µm. The planar scan configuration uses an oscillating linear scan head at rates of up to 10 Hz. The volume scan configuration uses the standard scan head attached to an XY gantry. Scan time is ~100 pixels/sec, meaning a 100 x 100 pixel scan takes ~2 min.

Processing: The Picometrix® control software implements many of the signal processing techniques commonly used with THz TDS systems to reduce noise [Ferguson and Abbott 2001]. TDS systems commonly record multiple waveforms and average them together to reduce the effects of background noise, at the expense of slower scan rates. Other common techniques include high/low pass filters and deconvolution using a reference and noise signal. We typically average five waveforms during the recording process and apply both high pass and low pass filters to improve signal quality. Once the scan data is recorded, it is analyzed offline using the *ImageJ* scientific image processing package (`imagej.nih.gov/ij`) with custom plugins written in Java. Realtime processing can currently be performed using the ray and planar scan configurations; we envision future TDS systems will support realtime volume scanning.

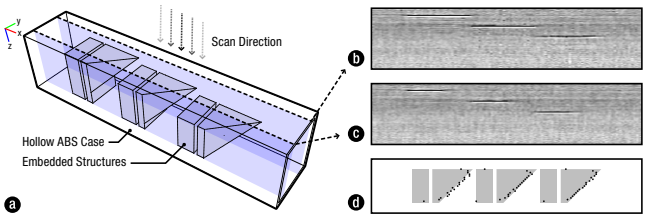

Figure 9: *(a) Geometric structures embedded inside an ABS case are imaged with a THz planar scan system. (b-c) Horizontal position information is recovered by measuring the changing size of reflections off the embedded structures. (d) The measured size of reflections plotted against the top view of the internal geometry.*

5.3 InfraStruct Results

We now describe details of the fabrication, imaging, and testing of our prototype *InfraStruct* tags.

Gray Code: The Gray code tag design is created from 10 layers of 127 µm clear polystyrene, five layers each for X and Y encoding (Figure 8a,b). The material layers are mechanically aligned in a 3D printed ABS case with a 3.18 mm cover layer of white HDPE to maximize THz penetration. Figure 8c shows a ray scan signal that has successfully been decoded. We design the Gray code structure to gracefully degrade if there is signal loss, by interlacing the X and Y patterns: $\{X_1, Y_1, X_2, Y_2 ... X_n, Y_n\}$. Higher order bits are positioned closer to the object exterior to ensure minimal signal attenuation. In cases where $X_1 ... Y_n$ of the signal is not returned due to attenuation, the first part of the signal still resolves to a lower resolution location reading (Figure 8d). As Gray codes have a $log_2(n)$ relationship between the number of patterns and the number of resolvable pixels, n, lower bit failures degrade gracefully.

Geometric: The geometric tag design consists of pyramid-like structures embedded inside a hollow tube (Figure 9a). The prototype is fabricated from ABS using an FDM Stratasys Dimension SST 1200es 3D printer with a wall thickness of 1mm and 10mm wide pyramid structures. The pyramid structures are designed to reflect distinct signals from a top-down planar scan that cuts through the object. Figure 9b and 9c show signal amplitude data mapped to image slices at two locations in the tube. The length of the reflections from the pyramid structures is used to determine the location at which the planar scan intersects the tube. The height of the pyramid structures determines the 180°orientation of the tube, i.e., facing left or right. Planar scan data from the outer surface of the tube enables recovery of the X and Z location as well as limited Y rotation. To calculate the accuracy of reflections from the internal structure, we captured 19 planar scans intersecting the pyramid structures at regular intervals from edge to edge. Each planar scan was mapped to an image and processed to measure the length of the three internal reflections compared to the known distance. Figure 9d shows the measurement results plotted to scale on the top view of the internal geometry. For all samples the average error was 0.93 mm (SD = 2.82 mm). However, it is clear that the data near the edges of the pyramid is unreliable due to signal loss. Ignoring the two edge datasets results in an average error of 0.13 mm (SD = 0.67 mm).

Random Void: The random void tag design consists of a photopolymer resin model, created on a Objet Eden 350V 3D printer, with 100 air pockets randomly distributed across the face of the 50 x 75 x 7.5 mm object (Figure 10a). The internal voids are 1.5 mm cubes with varying depth in the Z axis (0.8 - 5.2 mm). To determine if the tag could be used for object identification and pose estimation we captured 178 parallel planar scans along the length of the ob-

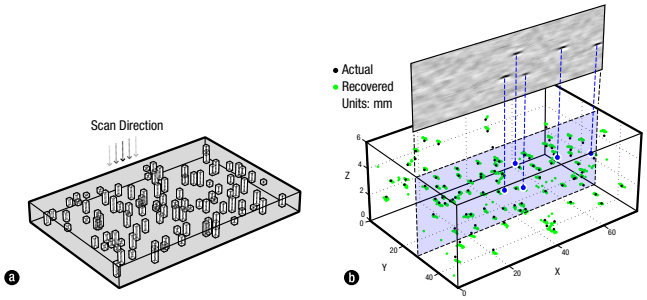

Figure 10: *(a) Randomly distributed voids are fabricated inside a 3D printed object. (b) Planar scan data is used to recover the location of voids and match them to a stored model. A single matched scan can be used for both object identification and pose estimation.*

ject. Image thresholding and connected components analysis was performed on the resulting images, with each connected component determined to be a void. An average of 4.9 voids were detected in each planar scan. After aligning the volumetric scan to the stored 3D model, the recovered position was matched to the nearest void in the model. Figure 10b shows that all voids were successfully detected with an average positional error of 0.9 mm (SD = 0.7 mm). A single scan image illustrates the data being matched.

To test whether a single planar scan can be reliably aligned to the model, we assumed the rotation about the Z axis and XY translation with respect to the model were unknown. This simulates a realistic scenario where the distance to surface and surface normal is known, but scan position and rotation about the normal are unknown. An exhaustive search over all such rotations and translations was performed to find the closest match between the detected voids and the model. We defined a match score as the sum of the distance, over all detected voids, to the nearest void in an 8mm wide slice of the rotated and translated model. In this simulation, a correct alignment should result in a minimum match score at zero translation and rotation. We found 154 of the 178 scans (87%) were correctly aligned. Of the 24 incorrectly aligned scans, 7 were caused by spurious void detections and 15 by insufficient voids for matching (<4). Scan length and feature density can be tuned to application requirements, e.g., improved accuracy.

Matrix: The matrix tag design is created from three layers of 794 µm thick white polystyrene enclosed within a 3D printed ABS case (Figure 11a). Embedded bit patterns are laser cut from the polystyrene to make up a 3 x 3 x 3 volumetric grid. A 1 mm frame is left in place around each cut to ensure mechanical stability. The

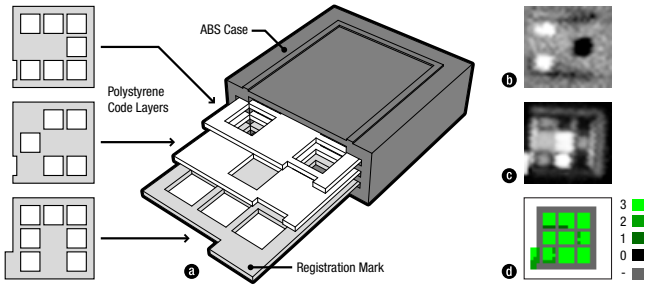

Figure 11: *(a) A matrix of binary data is encoded into three layers of laser-cut polystyrene. (b) Time-domain image slice. (c) Maximum image calculated from the volumetric image. (d) Pixel-by-pixel read-accuracy in bits.*

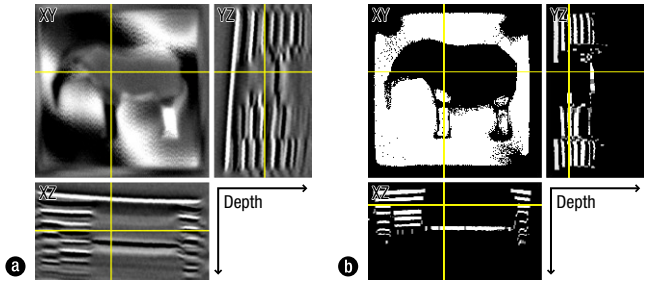

Figure 12: *(a) A volume scan of a layered 3D watermark in the shape of an elephant. TOF measurements through different materials result in layer misalignment. (b) We realign the layers by detecting material transitions then binarize the image.*

bottom layer has a registration mark used to orient the code correctly. Several measures are implemented to ensure robust signal decoding. Firstly, 1mm air gaps are left between layers to allow the returned signal to settle between each reflection peak. Secondly, the bottom layer is lined with an opaque metallic film to ensure a strong reflection. These additional measures aid in decoding the signal without the need for typical de-noising techniques.

A low resolution 30 x 30 x 4096 scan was taken of the matrix tag design using a volume scan configuration. Figure 11 shows (b) a time-domain image slice and (c) the maximum image from the volumetric dataset. The scan data was processed to extract the binary information using our standard algorithm on each waveform and checked for accuracy. Each of the 27 bits were successfully decoded as well as the extra registration mark. For the entire scan a total of 603 bit states were recorded with 567 read correctly (94% accuracy). Figure 11d shows the results of the pixel-by-pixel accuracy for the scan. Failure cases were encountered at the edges of each bit-slot. Although we use a binary encoding scheme, additional dimensions of encoding can be implemented in a matrix tag, such as varying material thickness or reflectivity. More advanced encoding schemes may look to utilize an error correction scheme such as Reed-Solomon [MacKay 2003].

Visual: The visual tag design consists of five 254 µm layers of white polystyrene depicting slices though a 3D elephant model (Figure 13, top). Shapes are laser cut from each layer and the structure is enclosed inside a 3D printed ABS case. Figure 12a illustrates three cross-sections created from a volume scan of the prototype tag. Sections are indicated by yellow lines. The XY image shows the positive and negative reflections scrolling across the surface as it is not entirely flat. The YZ image shows the layered internal structure of the watermark at a slightly offset angle. The XZ image shows how TOF measurements through different materials result in

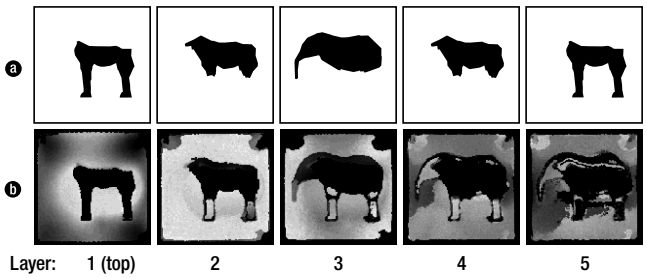

Figure 13: *By realigning the TOF measurements in a THz volume scan we can reconstruct (b) the shape of the original layers (a). Signal transitions near the shape edges are the main cause of error.*

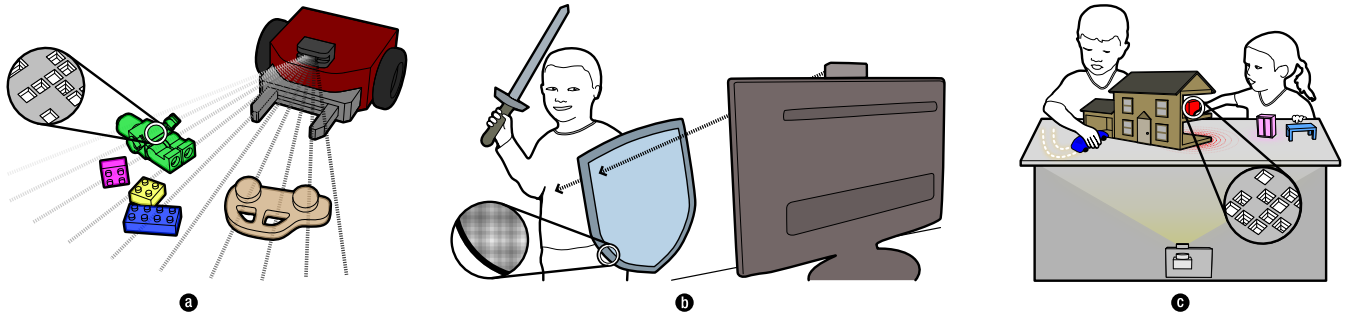

Figure 14: *Potential future applications for InfraStruct tags: (a) Mobile robots with THz range finders that also recognize objects in the environment, (b) customized game accessories with embedded tags for location sensing and the ability to image occluded parts of the user, (c) tabletop computing with tangible objects sensed through other objects beneath them.*

layer misalignment. As light travels much faster through air than plastic, hollow areas, such as the body of the elephant, return a signal before other areas.

Layer misalignment can be resolved in several steps provided the material refractive index is known. We first search for material transitions in each time-domain signal. We assume areas of the signal between a strong negative entry peak and a strong positive exit peak are inside a layer of material. We scale these areas of the signal down by a factor of the refractive index and binarize them to indicate they contain material. Other areas of the signal are binarized without scaling to indicate they contain air. Figure 12b shows three binary cross-section views of Figure 12a with our realignment algorithm applied. To recover images of each layer we firstly apply a median filter to each binary XY image slice to remove signal noise. We then average the multiple XY image slices that contain a signal. Figure 13 shows the reconstructed layers created with this approach. The main source of error comes from signal transitions near the edges of each shape. This error is accumulative and causes the outlines of the upper layers to be present in all subsequent layers. However, as the source of the error is known, i.e., the shape of the upper layers, errors can be compensated to improve the image quality of lower layers.

6 Future Applications

As digital fabrication enables a wide range of physical forms to be created, we envision an equally wide range of possible applications for *InfraStruct* tags. Tag designs that support identification of digitally fabricated objects have immediate applicability in production line inventory and point of sale systems. For example, the ability to accurately identify individual 3D printed objects within a large batch can increase the efficiency of production logistics (Figure 1a). As *InfraStruct* tags do not require additional stickers or labeling for machine-readability, new opportunities arise for ecologically-friendly packaging.

InfraStruct tags can enable new applications for ubiquitous computing. Customized objects created with personal 3D printers can be identified and connected to the 'internet of things' as soon as they are fabricated. Robotics applications may look to utilize THz planar scan systems to not only reveal depth information, but also identify and track objects in the environment (Figure 14a). With future improvements in THz scanning technology we foresee many human-computer interaction applications. Gray code patterns can be embedded in customized game accessories to sense location with a single THz ray scan when within range (Figure 14b). Volume scan configurations can potentially image behind game accessories using the latter part of the THz signal. The see-through ability of THz can also extend tabletop computing scenarios where objects are stacked, buried, or inserted inside other objects, and would typically be occluded from conventional cameras (Figure 14c).

7 Discussion

Because THz imaging technology is still relatively immature, this work has a number of limitations that we now discuss. All measurements described in this section were performed on a Zomega Mini-Z system (`www.z-thz.com`) (Figure 15). The Mini-Z has a time resolution of 0.04 ps, equating to a depth resolution of 12 µm. Calibration pieces were fabricated on an Objet Eden 350V 3D printer from VeroGray material with a tolerance of 20-85 µm.

7.1 Angle

THz TDS systems rely on specular reflection from surfaces to register a signal. The Fresnel equations determine the angle at which THz radiation will reflect from a surface back into the system lens and on to the receiver. The key variables are the lens radius, r, and the distance to the surface, d. The maximum incident angle can be determined by:

$$a = \frac{\arctan(\frac{r}{d})}{2} \tag{4}$$

The Mini-Z system uses a 12.7 mm radius lens with a focal length of 25.4 mm for a maximum incident angle of 13.28°. We verified this with a 3D printed calibration piece and found a planar surface can be rotated +/-11° before the signal was indistinguishable from noise. Angle constraints can potentially be overcome by using dif-

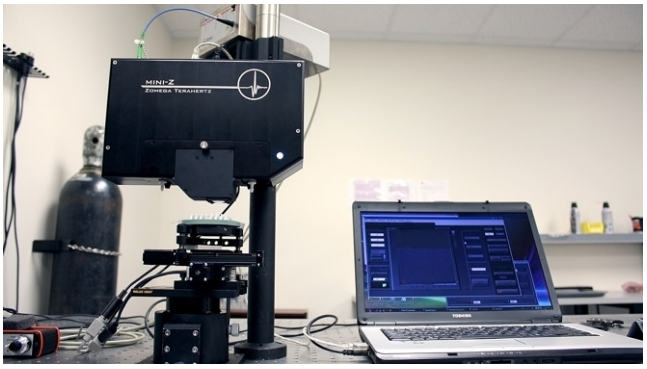

Figure 15: *The Zomega Mini-Z THz TDS system used with our experiments is roughly the size of a projector.*

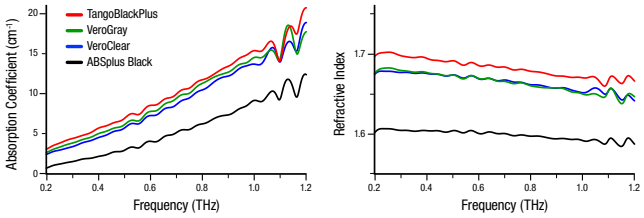

Figure 16: *The THz absorption coefficient (left) and refractive index (right) of several common 3D printer materials.*

fuse reflection instead of specular reflection. Diffuse reflection THz systems have been demonstrated and shown to achieve incident angles of between 35-55° [Liu et al. 2006]. However, diffuse reflection systems have a weaker return signal and require surface facets larger than THz wavelengths (30-3000 µm).

7.2 Depth

We performed measurements with a 3D printed calibration piece to determine the depth accuracy of a THz TDS system. The test piece consisted of 20 steps in 1000 µm increments. We measured the difference between each consecutive step for a mean value of 971 µm (SD = 98 µm). Although this equates to a high level of depth resolution, depth of field is currently narrow at around 20 mm. This limited working area is a result of the macro focusing optics used in most commercial TDS systems; larger focusing optics can be used to extend both focal point distance and depth of field. Although THz suffers from attenuation at distances greater than 10 meters [Armstrong 2012], many applications take place at much closer ranges.

7.3 Transmission

We found that limited data is available on the THz transmission properties of materials commonly used with 3D printing. To better understand transmission performance of 3D printed materials we measured the properties of: Objet *TangoBlackPlus*, *VeroGray*, *VeroClear*, and Stratasys *ABSplus Black*. A two mm thick sample of each material was measured using a TDS system in transmission mode. The refractive index and absorption coefficient of each material is shown in Figure 16.

The results show the three Objet photopolymer resin materials have a very similar response. When used with a TDS system, the limited difference in refractive index will result in a weak reflection at interfaces between these materials. We did observe a limited signal reflected back from transitions between the soft *TangoBlackPlus* material and the rigid *VeroGray* material in a multi-material print. However, far stronger signals were achieved with the equivalent transition from air to *VeroGray*. Although the ABS plastic was the least attenuating material, we encountered issues imaging through thick sections of ABS created with the FDM process where thin layers of plastic are thermally fused together in a lattice-like pattern. A cross-section of a 'solid' wall created on a Stratasys Dimension SST 1200es reveals gaps on the order of 200 µm (Figure 17). These gaps likely cause scattering at some THz wavelengths.

Figure 17: *The internal structure of a 'solid' wall made with an FDM 3D printer has gaps on the order of 200 µm. This irregular structure likely causes THz radiation to scatter inside.*

7.4 Safety and Privacy

THz waves have low photon energies that do not cause harmful photoionization in biological tissues and are generally considered to be safe for humans [Orlando and Gallerano 2009]. Current THz systems typically have a maximum emission power of a few µW. Safety standards for THz radiation are outlined in both the RF and laser standards with maximum permissible exposure values specified [Berry et al. 2003]. As THz radiation can penetrate many common textiles, privacy is a consideration for applications that scan the human body. Skin tissue is reflective and can potentially reveal human anatomy from beneath clothing. The ethics of using THz imaging for human interaction remains an issue to be addressed.

8 Conclusion

We have introduced the design, fabrication, imaging, and data processing of *InfraStructs*. Our prototype tag designs demonstrate how *InfraStructs* can be used for location encoding, pose estimation, object identification, data storage, and visual authentication.

We see numerous directions for future research. On the fabrication side, new 3D printing materials and technologies will play a key part in realizing physical objects with complex, data-filled internal structures. Dynamically mixing multiple materials for digitally controllable refractive indices will enable higher dimension data to be sensed and materials to be optimized for given data. On the imaging side, custom imaging devices will enable *InfraStructs* to be detected in a wider range of settings. Real-time volumetric scan systems will enable richer interaction scenarios, but also produce masses of data to be processed. Algorithms to process these huge datasets will be of key importance for future interactive systems.

The development of THz CMOS emitters [Huang et al. 2008] and detectors [Sherry et al. 2012] shows great potential to lower the price of THz imaging. Current trends towards faster electronics are forming a timely synergy with nano-fabrication technologies – enabling THz frequency electronics and the fabrication of THz wavelength-scale components. We foresee many exciting new applications at the interface between these two technologies.

References

ALEXA, M., AND MATUSIK, W. 2010. Reliefs as images. *ACM Trans. Graph. 29*, 4, 60:1–60:7.

ALIAGA, D. G., AND ATALLAH, M. J. 2009. Genuinity signatures: Designing signatures for verifying 3d object genuinity. In *Proc. EUROGRAPHICS*, 437–446.

ARMSTRONG, C. M., 2012. The truth about terahertz, September. `http://spectrum.ieee.org/aerospace/military/the-truth-about-terahertz`.

AUSTON, D. H., AND CHEUNG, K. P. 1985. Coherent time-domain far-infrared spectroscopy. *J. Optical Society of America B 2*, 4, 606–612.

BÄCHER, M., BICKEL, B., JAMES, D. L., AND PFISTER, H. 2012. Fabricating articulated characters from skinned meshes. *ACM Trans. Graph. 31*, 4, 47:1–47:9.

BERNIER, M., GARET, F., PERRET, E., DUVILLARET, L., AND TEDJINI, S. 2011. Terahertz encoding approach for secured chipless radio frequency identification. *Appl. Opt. 50*, 23, 4648–4655.

BERRY, E., WALKER, G. C., FITZGERALD, A. J., ZINOV EV, N. N., CHAMBERLAIN, M., SMYE, S. W., MILES, R. E., AND SMITH, M. A. 2003. Do in vivo terahertz imaging systems comply with safety guidelines? *J. Laser Applications 15*, 3, 192–198.

BICKEL, B., BÄCHER, M., OTADUY, M. A., LEE, H. R., PFISTER, H., GROSS, M., AND MATUSIK, W. 2010. Design and fabrication of materials with desired deformation behavior. *ACM Trans. Graph. 29*, 4, 63:1–63:10.

CHAN, W. L., DEIBEL, J., AND MITTLEMAN, D. M. 2007. Imaging with terahertz radiation. *Reports on Progress in Physics 70*, 8, 1325–1379.

CHAO, Y.-L., AND ALIAGA, D. G. 2013. Hiding a second appearance in a physical relief surface. In *Information Hiding*, M. Kirchner and D. Ghosal, Eds., vol. 7692 of *Lecture Notes in Computer Science*. Springer, 94–109.

FERGUSON, B., AND ABBOTT, D. 2001. De-noising techniques for terahertz responses of biological samples. *Microelectronics Journal 32*, 12, 943–953.

HASHEMI, H. 1993. The indoor radio propagation channel. *Proc. IEEE 81*, 7, 943–968.

HAŠAN, M., FUCHS, M., MATUSIK, W., PFISTER, H., AND RUSINKIEWICZ, S. 2010. Physical reproduction of materials with specified subsurface scattering. *ACM Trans. Graph. 29*, 4, 61:1–61:10.

HIGHTOWER, J., BORIELLO, G., AND WANT, R. 2000. Spoton: An indoor 3d location sensing technology based on RF signal strength. CSE Report 2000-02-02, University of Washington.

HUANG, D., LAROCCA, T., CHANG, M.-C., SAMOSKA, L., FUNG, A., CAMPBELL, R., AND ANDREWS, M. 2008. Terahertz CMOS frequency generator using linear superposition technique. *IEEE J. Solid-State Circuits 43*, 12, 2730–2738.

KATO, H., AND TAN, K. 2007. Pervasive 2d barcodes for camera phone applications. *IEEE Pervasive Computing 6*, 4, 76–85.

KLEINE-OSTMANN, T., KNOBLOCH, P., KOCH, M., HOFFMANN, S., BREEDE, M., HOFMANN, M., HEIN, G., PIERZ, K., SPERLING, M., AND DONHUIJSEN, K. 2001. Continuous-wave thz imaging. *Electronics Letters 37*, 24, 1461–1463.

LIU, H.-B., CHEN, Y., BASTIAANS, G. J., AND ZHANG, X.-C. 2006. Detection and identification of explosive rdx by thz diffuse reflection spectroscopy. *Optics Express 14*, 1, 415–423.

LOPES, A. J., MACDONALD, E., AND WICKER, R. B. 2012. Integrating stereolithography and direct print technologies for 3d structural electronics fabrication. *Rapid Prototyping Journal 18*, 2, 129–143.

MACKAY, D. J. 2003. *Information Theory, Inference, and Learning Algorithms*. Cambridge University Press.

MOHAN, A., WOO, G., HIURA, S., SMITHWICK, Q., AND RASKAR, R. 2009. Bokode: imperceptible visual tags for camera based interaction from a distance. *ACM Trans. Graph. 28*, 3, 98:1–98:8.

NAKAZATO, Y., KANBARA, M., AND YOKOYA, N. 2008. Localization system for large indoor environments using invisible markers. In *Proc. VRST*, ACM, 295–296.

ORLANDO, A. R., AND GALLERANO, G. P. 2009. Terahertz radiation effects and biological applications. *J. Infrared, Millimeter and Terahertz Waves 30*, 1308—1318.

PAPPU, R., RECHT, B., TAYLOR, J., AND GERSHENFELD, N. 2002. Physical one-way functions. *Science 297*, 5589, 2026–2030.

PARK, H., AND PARK, J.-I. 2004. Invisible marker tracking for AR. In *Proc. ISMAR*, IEEE, 272–273.

RASKAR, R., BEARDSLEY, P., VAN BAAR, J., WANG, Y., DIETZ, P., LEE, J., LEIGH, D., AND WILLWACHER, T. 2004. RFIG lamps: Interacting with a self-describing world via photosensing wireless tags and projectors. *ACM Trans. Graph. 23*, 3, 406–415.

SALVI, J., PAGÈS, J., AND BATLLE, J. 2004. Pattern codification strategies in structured light systems. *Pattern Recognition 37*, 4, 827–849.

SHERRY, H., GRZYB, J., ZHAO, Y., AL HADI, R., CATHELIN, A., KAISER, A., AND PFEIFFER, U. 2012. A 1kpixel CMOS camera chip for 25fps real-time terahertz imaging applications. In *Proc. ISSCC '12*, IEEE, 252–254.

STAVA, O., VANEK, J., BENES, B., CARR, N., AND MĚCH, R. 2012. Stress relief: improving structural strength of 3d printable objects. *ACM Trans. Graph. 31*, 4, 48:1–48:11.

SUBRAMANIAN, V., FRECHET, J., CHANG, P., HUANG, D., LEE, J., MOLESA, S., MURPHY, A., REDINGER, D., AND VOLKMAN, S. 2005. Progress toward development of all-printed RFID tags: Materials, processes, and devices. *Proc. IEEE 93*, 7, 1330–1338.

TONOUCHI, M. 2007. Cutting-edge terahertz technology. *Nature Photonics 1*, 2, 97–105.

VELTEN, A., WILLWACHER, T., GUPTA, O., VEERARAGHAVAN, A., BAWENDI, M. G., AND RASKAR, R. 2012. Recovering three-dimensional shape around a corner using ultrafast time-of-flight imaging. *Nature Communications 3*.

WANG, S., AND ZHANG, X.-C. 2004. Pulsed terahertz tomography. *Journal of Physics D: Applied Physics 37*, 4, R1.

WEISER, M. 1993. Ubiquitous computing. *IEEE Computer 26*, 10, 71–72.

WEYRICH, T., PEERS, P., MATUSIK, W., AND RUSINKIEWICZ, S. 2009. Fabricating microgeometry for custom surface reflectance. *ACM Trans. Graph. 28*, 3, 32:1–32:6.

WILLIS, K. D. D., BROCKMEYER, E., HUDSON, S. E., AND POUPYREV, I. 2012. Printed Optics: 3D printing of embedded optical elements for interactive devices. In *Proc. UIST '12*, ACM, 589–598.

YANG, Y., AND FATHY, A. 2005. See-through-wall imaging using ultra wideband short-pulse radar system. In *Proc. Antennas and Propagation Soc. Int. Symp.*, vol. 3B, IEEE, 334–337.

YANG, L., RIDA, A., VYAS, R., AND TENTZERIS, M. 2007. RFID tag and RF structures on a paper substrate using inkjet-printing technology. *IEEE Trans. Microwave Theory and Techniques 55*, 12, 2894–2901.